

<https://doi.org/10.1038/s42003-024-06071-2>

The nuclear import receptor Kap β 2 modifies neurotoxicity mediated by poly(GR) in C9orf72-linked ALS/FTD

Check for updates

M. E. Cicardi¹, V. Kankate¹, S. Sriramoji¹, K. Krishnamurthy¹, S. S. Markandaiah¹, B. M. Verdone¹, A. Girdhar², A. Nelson¹, L. B. Rivas¹, A. Boehringer¹, A. R. Haeusler¹, P. Pasinelli¹, L. Guo²✉ & D. Trotti¹✉

Expanded intronic G₄C₂ repeats in the *C9ORF72* gene cause amyotrophic lateral sclerosis (ALS) and frontotemporal dementia (FTD). These intronic repeats are translated through a non-AUG-dependent mechanism into five different dipeptide repeat proteins (DPRs), including poly-glycine-arginine (GR), which is aggregation-prone and neurotoxic. Here, we report that Kap β 2 and GR interact, co-aggregating, in cultured neurons in-vitro and CNS tissue in-vivo. Importantly, this interaction significantly decreased the risk of death of cultured GR-expressing neurons. Downregulation of Kap β 2 is detrimental to their survival, whereas increased Kap β 2 levels mitigated GR-mediated neurotoxicity. As expected, GR-expressing neurons displayed TDP-43 nuclear loss. Raising Kap β 2 levels did not restore TDP-43 into the nucleus, nor did alter the dynamic properties of GR aggregates. Overall, our findings support the design of therapeutic strategies aimed at up-regulating Kap β 2 expression levels as a potential new avenue for contrasting neurodegeneration in C9orf72-ALS/FTD.

The most common genetic cause of amyotrophic lateral sclerosis (ALS) and frontotemporal dementia (FTD) is a non-coding G₄C₂ nucleotide repeat expansion (NRE) in the first intron of the *C9ORF72* gene (C9)^{1–3}. This NRE can be aberrantly translated through a process known as repeat-associated non-AUG translation (RAN-T), leading to the production of five different dipeptide repeat proteins (DPRs): poly glycine-alanine (GA), poly glycine-proline (GP), poly glycine-arginine (GR), poly proline-alanine (PA), and poly proline-arginine (PR)⁴. The arginine-rich DPRs, GR and PR, are the most neurotoxic, possibly in a length-dependent manner^{5,6}. Studies in in-vitro models have identified dysregulated pathways associated with the accumulation of GR and PR, such as translation stalling, stress granules persistence, nucleolar stress, DNA damage, and nuclear pore complex defects^{7–11}. A well-known pathological hallmark of most forms of ALS/FTD, including C9-ALS/FTD¹², is the mislocalization of TDP-43 from the nucleus, where it usually resides, to the cytoplasm. Expression of long GR dipeptides (≥ 200) in cells causes TDP-43 nuclear depletion and accumulation of cytoplasmic TDP43 inclusions¹². GR₈₀-expressing mice show behavioral impairments but lack TDP-43 mislocalization in neurons¹³. Also, our recently established mouse model, which constitutively expresses GR₅₀, develops mild motor behavioral phenotype⁶ but fails to display TDP-43

mislocalization in neurons. Interestingly, it showed disrupted nuclear pore complex integrity revealed in aged mice by Nup62 (nuclear pore complex protein) mislocalization in the cytoplasm¹⁴. From a mechanistic perspective, the influence of GR on nuclear import/export machinery remains unclear. Vanneste et al. showed that in-vitro expression of DPRs did not affect the nuclear import/export processes¹⁵, while Hayes et al. showed that R-rich DPRs disrupted the karyopherin-dependent nuclear import in a dose-dependent fashion¹⁶. Hutten et al., addressing specifically TDP-43 shuttling, showed that GR, even at a short length (GR₂₀), hinders TDP-43 nuclear import¹⁷. In line with this evidence, it was demonstrated that GA can specifically cause TDP-43 nuclear import defects¹⁸. TDP-43 mislocalization is strictly a neuronal event, at least in the human disease context. However, these last two studies were conducted in human cancer cell lines (HeLa), whose protein and RNA composition greatly varies from neuronal cells.

The GR interactome is composed of many proteins, most of which feature low complexity domains, through which the interaction with GR occurs, including RNA-binding proteins (RBPs), nucleolar components, stress granules components, and proteins involved in nuclear transport^{19,20}. Among the latter is karyopherin β 2 (Kap β 2, also known as transportin-1 or Importin β 2), which belongs to the family of nuclear import receptors

¹Weinberg ALS Center, Vickie and Jack Farber Institute for Neuroscience, Department of Neuroscience, Thomas Jefferson University, Philadelphia, PA, USA. ²Department of Biochemistry and Molecular Biology, Thomas Jefferson University, Philadelphia, PA, USA. ✉e-mail: lin.guo@jefferson.edu; davide.trotti@jefferson.edu

(NIRs) that orchestrate the exchange of proteins between the nucleus and cytoplasm²¹. The flow direction depends upon the asymmetric distribution of RanGTP/RanGDP between the nucleus and cytoplasm. Kapβ2 translocates to the nuclear envelope^{22,23}, where it can gain entry into the nucleus through interaction with the FG-Nups on the nuclear pore²⁴⁻²⁷. With this shuttling mechanism, Kapβ2 favors its entry into the nucleus when bound to its partners. Once in the nucleoplasm, Kapβ2 releases its cargo and relocates to the cytoplasm, freely transiting through the FG barrier of NPC channels while binding with the highly concentrated RanGTP. Once there, GTP is dephosphorylated in GDP, and Ran protein loses the interaction with Kapβ2, which is then ready for a new import cycle^{21,25,28-30}.

Even though no ALS-causative mutations in the *KAPB2* gene have been identified thus far, the Kapβ2 protein interacts with many ALS-causative proteins such as FUS, but also TAF, EWS, hnRNPA1, and hnRNPA2³¹⁻³⁴. Interestingly, the domain of these proteins involved in the interaction with Kapβ2 is a PY-NLS, a nuclear localization signal in which one proline (P) is followed by one tyrosine (Y), in which many of the most common and aggressive ALS-related mutations are found¹⁵⁻³⁷. Even at very short lengths (e.g., 10 repeats), GR is predicted to interact with Kapβ2 *via* the same domain¹⁶. A recent study shows that PR also interacts with Kapβ2 through the sites that recognize the PY-NLS³⁸. To add importance to the interaction of R-rich DPRs and Kapβ2, previous studies in yeasts showed that overexpression of KAP104, the yeast homolog of Kapβ2, decreased PR toxicity³⁹, while in flies, Kapβ2 RNAi worsens PR neurotoxicity^{19,40}.

In this work, we reported that GR interacts with Kapβ2 in primary neurons and CNS tissues, suggesting the relevance of this interaction to disease. We also explored the impact of this interaction on neuronal survival. Indeed, reduced levels of Kapβ2 had an adverse effect on the survival of neurons expressing GR. Conversely, increased Kapβ2 significantly mitigated GR neurotoxicity. These results indicate that Kapβ2 could be a modifier of a pathogenic disease mechanism. Therefore, manipulating its expression levels in neurons might be harnessed to design future therapies to improve their survival in C9orf72-linked neurodegeneration.

Results

Expression of GR does not alter endogenous levels of Kapβ2 in neurons

Recruitment of essential constituents of the translational machinery by GR can lead to translation stalling, affecting the expression levels of certain proteins⁴¹. Thus, we first investigated whether the expression of GR could potentially affect Kapβ2 protein levels in our experimental models. For experiments in cortical neurons, we employed a lentivirus expression vector that encodes GR₅₀ with Flag and GFP tags fused to the dipeptide N- and C-terminus, respectively, to aid with its visualization and identification when the encoding vector is transduced in cells. In addition, the lentivirus expression vector is driven by the neuronal-specific human synapsin promoter (hSyn). This promoter is active in neurons and will only drive gene expression in these cell types. In cortical neurons transduced with GR₅₀,

Fig. 1 | GR does not affect Kapβ2 levels in neurons.

a qPCR analysis of Kapβ2 levels in cortical neurons transduced with GFP or GR₅₀. Data are represented as mean ± S.E.M. (n = 6 biological replicates, Student *t*-test, n.s. not significant). **b** Homogenates of cortical neurons transduced with GFP or GR₅₀ were resolved on western blot (WB) and probed for GFP and Kapβ2. Total protein staining was used as the loading control. For cortical neuron transduction experiments, we employed a lentivirus expression vector that encodes GR₅₀ with Flag and GFP tags fused to the dipeptide N- and C-terminus, respectively. **c** The graph bar shows the quantification of the WB of cortical neuron extracts for Kapβ2 protein. Total protein staining was used to normalize. Data are represented as mean ± S.E.M. (n = 3 biological replicates, Student *t*-test, n.s. not significant). **d** qPCR analysis of Kapβ2 transcript levels in the cortex and spinal cord of GFP and GR₅₀-GFP mice. Data are represented as mean ± S.E.M. (n = 3 biological replicates, One Way-ANOVA, n.s.) **e** Western blot of cortex and spinal cord homogenates from GFP and GR₅₀ mice. GR₅₀ is Flag and GFP tagged at the N- and C-termini, respectively. Blots were probed for GFP and Kapβ2. Total protein staining was used as the loading control and normalizer. Data are represented as mean ± S.E.M. (n = 3 biological replicates, One Way-ANOVA, n.s.). **f** Western blot of cortex and spinal cord homogenates. Total protein staining was used as the loading control and normalizer. Data are represented as mean ± S.E.M. (n = 3 biological replicates, One Way-ANOVA, n.s.). **g** Western blot of controls and C9orf72 patient post-mortem cortex extracts. Total protein staining was used as the loading control. **h** Quantification of Kapβ2 expression levels in controls and C9orf72 patient post-mortem cortex extracts as normalized protein fold change. Data are represented as mean ± S.E.M. (n = 3 biological replicates, Student *t*-test, n.s. not significant).

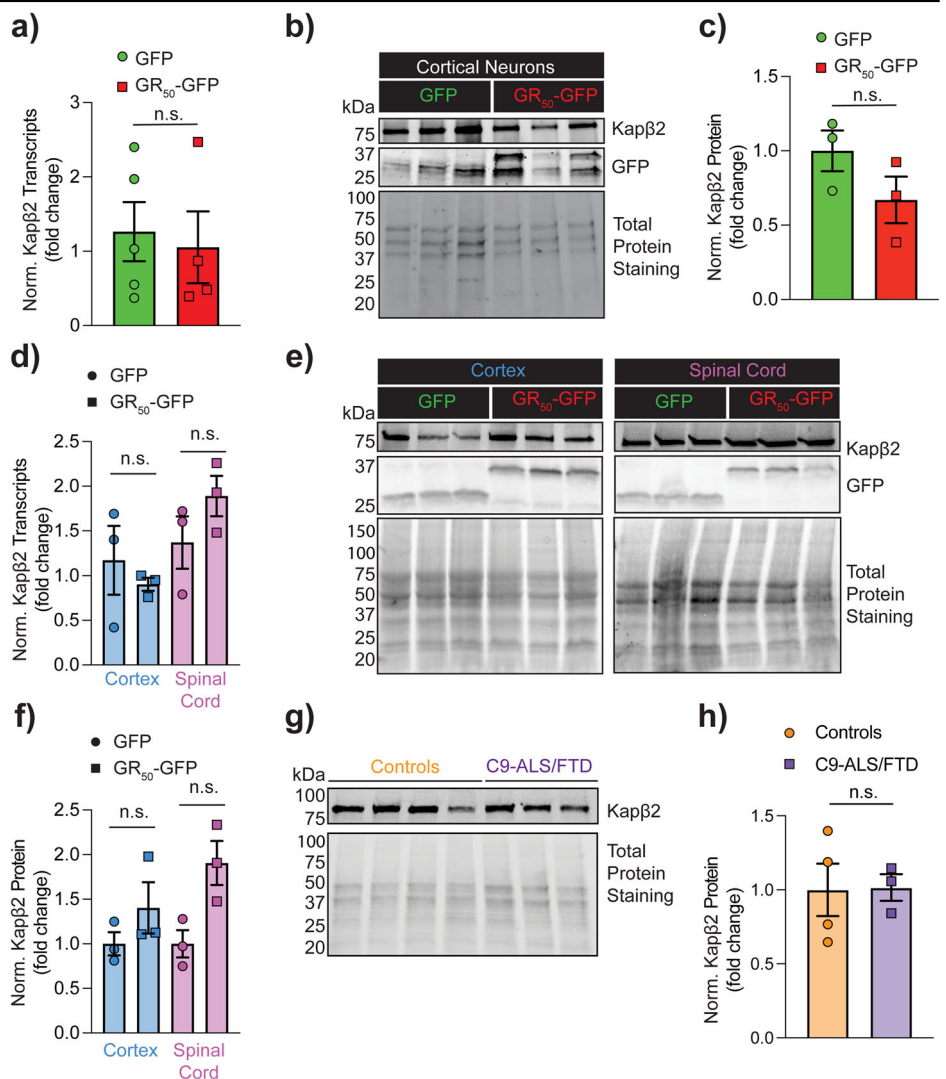
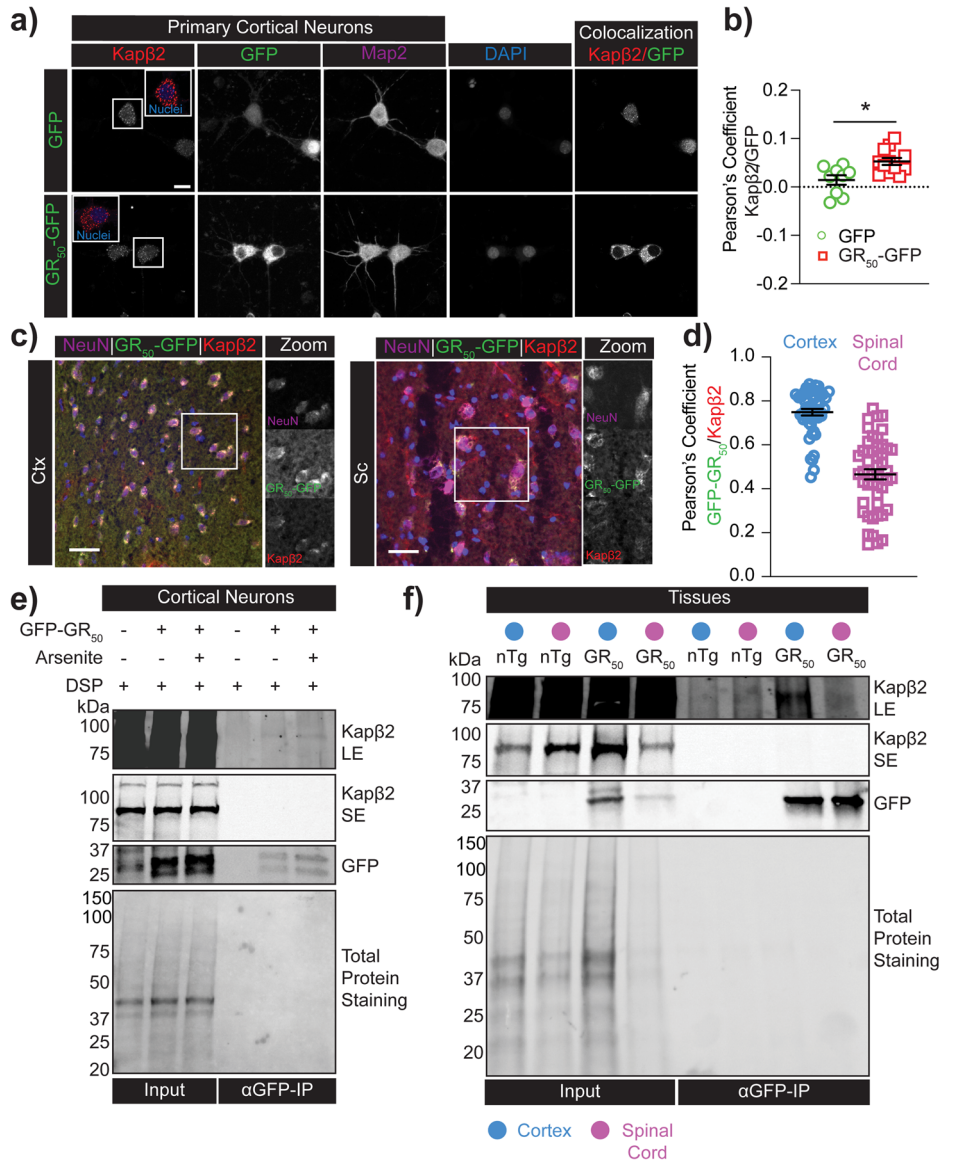


Fig. 2 | GR interacts and recruits Kapβ2 in neurons. **a** Confocal images of rat cortical neurons in culture transduced with GFP and GR₅₀ and stained for Kapβ2 and Map2. Imaris colocalization channel shows the amount of GFP colocalized with Kapβ2. Scale bar = 10 μm. **b** Pearson's coefficient measured in each neuron transduced with the lentivirus GR₅₀ construct (Flag-GR₅₀-GFP). Data are represented as mean ± S.E.M. (n = 3 biological replicates, m > 5 neurons, Student *t*-test, **P* < 0.05). **c** Confocal images of the cortex and spinal cord tissues of GR₅₀ mice stained for Kapβ2. Green is GFP reporting for GR₅₀, red is Kapβ2, and magenta is NeuN. Imaris colocalization shows the amount of GFP colocalized with Kapβ2. Scale bar = 30 μm. **d** Pearson's coefficient measured in the cortex and spinal cord neurons of GR₅₀ mice. Data are represented as mean ± S.E.M. (n = 3 biological replicates, m > 15 neurons). **e** Western blot analysis of the immunoprecipitation assay was performed in rat cortical neurons transduced with GR₅₀ and treated with arsenite (0.5 mM; 30 min). Blots were probed for GFP and Kapβ2. Total protein staining was used as the loading control. SE short exposure time, LE long exposure time. **f** Western blot of the immunoprecipitation assay performed in the cortex or spinal cord tissue of nTg or GR₅₀ mice. Blots were probed for GFP and Kapβ2. Total protein staining was used as the loading control. SE short exposure time, LE long exposure time.



there was no significant change in Kapβ2 mRNA compared to neurons expressing GFP used as reference (Fig. 1a, b; Supplementary Fig. 8). When we measured Kapβ2, we observed a trend in reduction in Kapβ2 protein levels in samples transduced with GR₅₀ compared to GFP alone, which did not reach statistical significance (Fig. 1c).

Moreover, we assessed Kapβ2 mRNA and protein levels in the cerebral cortex and spinal cord homogenates obtained from a transgenic mouse expressing GR₅₀ or GFP⁶. This analysis revealed no significant differences between the two groups in Kapβ2 mRNA and protein levels (Fig. 1d–f; Supplementary Fig. 8). We also assessed if there were discrepancies in the expression levels of the GR₅₀ and GFP transcripts. Still, we did not find significant changes between the experimental groups in cortical neurons and mouse CNS tissues (Supplementary Fig. 1a, b). While post-mortem tissues of C9orf72-ALS/FTD patients contain GR-positive aggregates, whose abundance varies in different brain regions⁴², we found that Kapβ2 protein expression levels were not changing, as determined by a western blot analysis of homogenates obtained from the motor cortex of C9orf72-ALS/FTD and non-diseased control cases (Fig. 1g, h; Supplementary Fig. 8). We also analyzed the expression of the Kapβ2 transcripts in publicly available datasets, including the one from the *Answer ALS consortium* (transcriptomic data from iPS-derived cortical neurons (iCN) from ALS patients) and the ALS Cell Atlas (frontal cortex and cerebellum transcriptomic data

from ALS patients and controls). We found no differences in Kapβ2 RNA transcript levels when comparing control and C9orf72-ALS/FTD groups (Supplementary Fig. 8c, d).

GR interacts with Kapβ2 in neurons

Earlier investigations utilizing pull-down assays revealed that Kapβ2 and GR interact in various human cell line models^{16,17}. To explore whether this interaction would also occur in cell types more relevant to the disease, we employed a lentivirus expression vector to transduce primary cortical neurons with GR₅₀ (Flag and GFP tagged). Immunofluorescence staining for Kapβ2 showed its perinuclear and cytoplasmic localization as expected (Fig. 2a). We also observed that GR₅₀ localization was predominantly cytoplasmic or perinuclear, similar to what we previously reported for our knock-in GR₅₀ (with Flag and GFP tags) mice⁶, where the expression of transgene is approximately at physiological levels. We then measured the Pearson's correlation coefficient in the cytoplasm of transduced neurons to evaluate whether GR₅₀ and Kapβ2 co-localize and estimated the degree of co-localization of these proteins in the same cellular compartments. Although the measured Pearson's coefficient yielded a low score, which verges on potential biological negligence according to the field⁴³, it's important to keep in mind that further analysis and interpretation may be required to determine its significance. Our analysis has shown that the

co-localization coefficient was higher in GR₅₀ neurons in comparison to neurons that were transduced with GFP. This indicates a stronger correlation between GR₅₀ and Kapβ2, as shown in Fig. 2b, than with GFP alone. Therefore, we interpret the low Pearson's coefficient score for the interaction of GR₅₀ with Kapβ2 as a reflection of the dynamic interaction between these two proteins. We measured the fluorescence of Kapβ2 in the nucleus and in the cytoplasm of neurons transduced with GR₅₀ and GFP alone. We observed a slight but non-significant decrease of Kapβ2 fluorescence in GR₅₀ compared to GFP samples, paralleled by a significant increase in cytoplasmic Kapβ2 fluorescence (Supplementary Fig. 2a). Plotting the nucleocytoplasmic ratio, we observed a substantial decrease in the GR₅₀ samples. This data suggests GR interferes with Kapβ2 localization in neurons, favoring its cytoplasmic localization.

Next, to investigate whether Kapβ2/GR also interacted in in-vivo models, we used a recently published GR₅₀ transgenic mouse model we generated and characterized⁶. This mouse model expresses Flag-GR₅₀-GFP predominantly in neurons. We first assessed the Kapβ2 localization pattern in wild-type, non-transgenic mice. We found that Kapβ2 mainly localized in perinuclear regions and cytoplasm of CNS cells (Supplementary Fig. 2b). We then performed Kapβ2 immunofluorescence staining in cerebral cortex and spinal cord sections of the GR₅₀ transgenic mouse employing Imaris software to perform 3D rendering and visualize the Kapβ2 localization in the cortex and spinal cord neurons. We found robust co-localization of Kapβ2 and GR₅₀ (Pearson's coefficient ranging between 0.5 and 1 in both tissues) in NeuN-positive cells (Fig. 2c, d; Supplementary Fig. 2c; Supplementary Movie 1). We also observed a higher Pearson's coefficient in cortical neurons than in motor neurons, possibly due to the different expression levels of Kapβ2 in the two cell types (<https://www.proteinatlas.org/ENSG00000083312-TNPO1>).

Further confirmation for GR₅₀ and Kapβ2 reciprocal interaction in neurons and CNS tissues came from co-IP experiments. However, this assay posed a challenge, as the fluorescent GFP reporter interacts with numerous proteins in cells. A dataset containing over 2900 protein entries found to interact with both GFP and GR₅₀ was recently published⁴⁴ (MassIVE identifier MSV000088581) (Supplementary Fig. 3a). We plotted the intensities of the interacting proteins and found that Kapβ2 and Kapβ2b were significantly enriched in the GR₅₀ group compared to the GFP group (Supplementary Fig. 3b), suggesting that Kapβ2 and GR₅₀ could be interacting partners. To further study this interaction, we carried out co-IP in GR₅₀ transduced cortical neurons. Before harvesting the neurons, we treated the sample with the crosslinker DSP to preserve even the most dynamic and transient interactions between these two proteins. In immunoprecipitates from neurons expressing GR₅₀, we observed Kapβ2. Its interaction with GR₅₀ increased in neurons treated with the cellular stressor, arsenite (Fig. 2e; Supplementary Fig. 8). We performed the same co-IP in control GFP-expressing neurons. As expected, a fraction of Kapβ2 was non-specifically bound to GFP, but a larger fraction was bound to GR₅₀ (Supplementary Fig. 3c, d). Kapβ2 and GR interaction was also confirmed by co-IP using anti-FLAG M2 agarose beads to pull down GR₅₀ (Supplementary Figs. 4a, 8). Finally, we conducted reverse co-IP experiments by using a Kapβ2 antibody to capture GR. Our results showed that a portion of GR was co-immunoprecipitated with Kapβ2, especially in arsenite-stressed neurons (Supplementary Figs. 4b, 8).

Co-IP experiments were also conducted in cortex and spinal cord lysates obtained from transgenic Flag-GR₅₀-GFP mice⁶. As seen in cultured neurons, Kapβ2 co-immunoprecipitated with GR₅₀ when we used an anti-GFP antibody but not in non-transgenic control CNS tissue lysates or when we used for co-IP the corresponding IgG control (Fig. 2f and Supplementary Figs. 4c, 8). In addition, we performed a reverse co-IP using a Kapβ2 antibody, which also revealed evidence of GR bound to Kapβ2 (Supplementary Figs. 4d, 8).

Kapβ2 is protective against GR-mediated neurotoxicity

Next, we conducted a study to investigate if the Kapβ2-GR interaction affects the toxicity of GR in neurons. Our goal was to diminish the

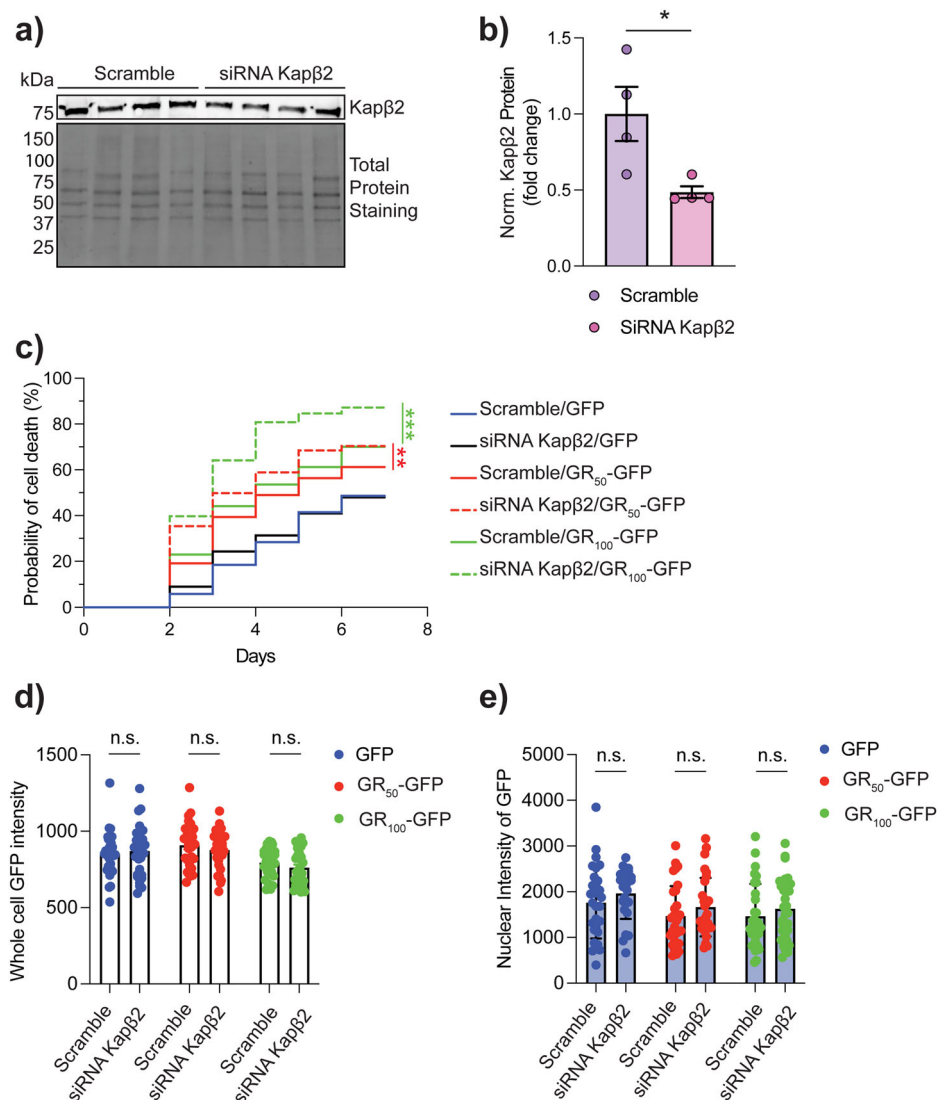
expression of Kapβ2 in neurons that express GR and document its impact on their survival. To achieve this, we used a combination of 4 siRNAs that specifically target Kapβ2 RNA transcripts. The transfection of these siRNAs resulted in a substantial decrease of Kapβ2 protein levels by approximately 50% after 48 h (Fig. 3a, b; Supplementary Fig. 8). Using live-cell imaging microscopy, we measured a significant reduction in viability in the GR₅₀ and GR₁₀₀ (GFP tagged) expressing neurons in which Kapβ2 was silenced (Fig. 3c, Supplementary Fig. 5c, Supplementary Table 1). We measured the fluorescence intensity of GFP in all experimental groups 48 h after transfection to determine if Kapβ2 knockdown impacted the expression levels of GR₅₀ and GR₁₀₀. No difference was observed (Fig. 3d) even when we looked at the nuclear accumulation of GR₅₀ and GR₁₀₀ (Fig. 3e), suggesting that Kapβ2 is not involved in GR degradation or subcellular localization. Similarly, knocking down Kapβ2 in neurons did not affect nuclear FUS levels, a known and extensively studied substrate for Kapβ2 and an ALS-causative protein when mutated³⁴, measured by quantifying the FUS immunofluorescence signal (Supplementary Fig. 8a, b). These results led us to hypothesize that increasing the levels of Kapβ2 might play a protective role against GR-mediated neurotoxicity.

Next, we co-expressed GFP-tagged Kapβ2 and GR₅₀₋₁₀₀-mCherry in primary cortical neurons to test the hypothesis that Kapβ2 plays a neuroprotective role and assessed the viability of the co-transfected neurons in culture. Heterologously expressed Kapβ2 localized in cytoplasmic puncta that mainly surrounded the nucleus of neurons (Fig. 4a, Supplementary Movie 2). We first determined that Kapβ2 or GFP alone were not toxic to neurons when heterologously expressed at two different DNA concentrations (400 and 800 ng/well) (Fig. 4b, c; Supplementary Fig. 6a, b; Supplementary Table 2). This suggested that elevating Kapβ2 expression does not adversely affect neuronal viability. Next, we expressed both Kapβ2 and GR₅₀ or GR₁₀₀ and assessed the overall risk of death of the transfected neurons. We kept a 1:1 DNA ratio of Kapβ2-GFP (or GFP alone as control) and GR-mCherry (or mCherry alone), and GFP/mCherry-positive neurons were imaged and analyzed over 8 days (Fig. 4d, e; Supplementary Fig. 6c; Supplementary Table 3). Expression of GR₅₀ or GR₁₀₀ in neurons increased their risk of death compared to their respective controls (mCherry vs. GR₅₀-mCherry $p < 0.0001$; mCherry vs. GR₁₀₀-mCherry $p < 0.0001$) as previously reported⁵⁶. However, co-expression of Kapβ2 in GR₅₀₋₁₀₀ (mCherry tagged) neurons reduced their overall risk of death to control levels (GR₅₀-mCherry vs. GR₅₀-mCherry/Kapβ2 $p < 0.0001$; GR₁₀₀-mCherry vs. GR₁₀₀-mCherry/Kapβ2 $p = 0.005$) (Fig. 4d, e; Supplementary Fig. 6c; Supplementary Table 3) indicating that Kapβ2 can indeed rescue neurons from the intrinsic toxicity of GR expression.

Kapβ2 exhibits localization to GR aggregates but doesn't affect GR aggregation propensity, GR aggregates dynamic properties, and GR localization pattern in neurons

To explore the mechanism by which Kapβ2 protects neurons from GR toxicity, we first evaluated whether Kapβ2 affected the formation and stability of GR aggregates. In neurons, the subcellular localization of GR₅₀ and GR₁₀₀ differs significantly. GR₅₀ is predominantly located in the nucleus, while GR₁₀₀ is mainly in the cytoplasm (Fig. 5a and Supplementary Fig. 6d). Despite both GR species form aggregates in the cytoplasm, with no observable difference in the number of aggregates per cell between GR₅₀ and GR₁₀₀ expressing neurons (Fig. 5e), we analyzed the intensity profile of GFP (reporting on the transfected Kapβ2) and mCherry (reporting on the transfected GRs) channels in the GR aggregates. We observed selective localization of Kapβ2 within aggregates, as opposed to cytoplasmic diffusion like GFP, as shown in Fig. 5a, b. Furthermore, the fluorescence intensity profile of the aggregates indicated that the recruitment of Kapβ2 was even higher in GR₁₀₀-expressing neurons, suggesting that Kapβ2 could ultimately affect GR localization. However, we found no difference in GR fluorescence within the nuclei in the presence of Kapβ2, as illustrated in Fig. 5c. Additionally, we found that the mean fluorescence of each aggregate remained constant when Kapβ2 was recruited into them, as shown in Fig. 5d. Kapβ2 did not alter

Fig. 3 | Silencing of Kapβ2 increases death risk in the presence of GR. **a** Western blot showing Kapβ2 expression in neurons treated with Smart pool siRNA (100 μM). Blots were probed for Kapβ2. Total protein staining was used as the loading control. **b** Kapβ2 levels in primary neurons treated with Smart pool siRNA 100 μM or scramble. Data are represented as mean ± S.E.M. (n = 3 biological replicates, Mann-Whitney non parametric test, $P < 0.05$). **c** The plot depicts the probability of neuronal death in each group via a cumulative risk of death plot. Time-lapse experiments on rat primary cortical neurons transfected with siRNA Kapβ2 100 μM or scramble and GFP, GR₅₀-GFP, or GR₁₀₀-GFP. (n = 3 biological replicates, m > 50 neurons, Log-rank Mantel-Cox test * $p < 0.05$, *** $p < 0.001$). **d** Quantification of the mean fluorescence of GFP expressing neurons 48 h after transfection in cells previously treated with Kapβ2 siRNA or scramble. Data are represented as mean ± S.E.M. (n = 3 biological replicates, m > 10 neurons, One-Way ANOVA, $p = n.s.$ not significant). **e** Quantification of the mean nuclear fluorescence of GFP expressing cells 48 h after transfection in cells previously treated with Kapβ2 siRNA or scramble. Data are represented as mean ± S.E.M. (n = 3 biological replicates, m > 10 neurons, One-Way ANOVA, $p = n.s.$ not significant).



the number of aggregates per cell for either GR species (Fig. 5e). Finally, by calculating the Pearson’s correlation coefficient to assess whether the recruitment and colocalization of Kapβ2 and GR depended on the repeat length, we found that GR₁₀₀ aggregates displayed a more substantial positive correlation value than GR₅₀ (Fig. 5f).

Kapβ2 affects the dynamic properties of FUS aggregates³⁷, as demonstrated by its ability to modulate their physical properties, liquid phase separation, and formation of insoluble gel-like structures³⁴. To investigate whether Kapβ2 similarly influences the GR aggregates, we co-expressed Kapβ2-GFP and GR₅₀ or GR₁₀₀-mCherry in cortical neurons and used fluorescence recovery after photobleaching (FRAP) to assess the overall fluidity of the aggregates (Fig. 6a–c; Supplementary Fig. 6e). We observed that the mCherry fluorescence recovery was significantly higher in GR₅₀-mCherry when compared to GR₁₀₀-mCherry aggregates. This observation led us to conclude that the aggregates formed by GR₁₀₀-mCherry were more stable (Fig. 6a–c). Notably, in the presence of Kapβ2-GFP, the fraction of mCherry fluorescence recovery remains unchanged for both GR₅₀-mCherry and GR₁₀₀-mCherry aggregates, suggesting that Kapβ2 does not bring the aggregates in a more dynamic and fluid state (Fig. 6d–h; Supplementary Fig. 6e). These findings indicate that Kapβ2 when co-aggregates with GR, does not alter the structure of the inclusions, confirming what shown in silico by ref. 17.

In the presence of GR, Kapβ2 is crucial in regulating TDP-43 localization, although it does not directly bind to TDP-43¹⁷. We

conducted experiments in vitro, in a test tube, where GR/TDP-43 aggregates were allowed to form in the presence and absence of Kapβ2. We used an equimolar concentration (5 μM) for all three proteins. When combined, GR and TDP-43 formed large condensates (Fig. 7a, Supplementary Fig. 7). It is interesting to note that the introduction of Kapβ2, but not an unrelated protein like BSA (5 μM), reduced the size of the aggregates, enriched TDP-43 within the aggregates, and increased the diffusive TDP-43 fluorescence signal outside the aggregates (as shown in Fig. 7b, c). This suggests that Kapβ2 made a portion of TDP-43 soluble. We then hypothesized that the fraction of TDP-43 freed from the aggregates by Kapβ2 would be available to re-enter the nucleus freely. This hypothesis was tested in primary rat neuronal cultures. We measured intranuclear TDP-43 in neurons co-transfected with GR_{50,100}-mCherry and Kapβ2-GFP or GFP as control and found that TDP-43 was significantly depleted from the nucleus of neurons expressing GR_{50,100} compared to GFP-expressing control neurons (Fig. 7d, e). Under this experimental condition, the expression of Kapβ2-GFP did not revert TDP-43 nuclear loss caused by the presence of GR. We thus analyzed TDP-43 content in GR aggregates, and as expected, we found that GR aggregates were enriched in TDP-43. However, we also found that the fraction of TDP-43 in the aggregates did not change in the presence of Kapβ2 (Fig. 7d–f). Overall, while in neurons Kapβ2 makes GR aggregates more dynamic, it does not influence TDP-43 relocation to the nucleus or the aggregates.

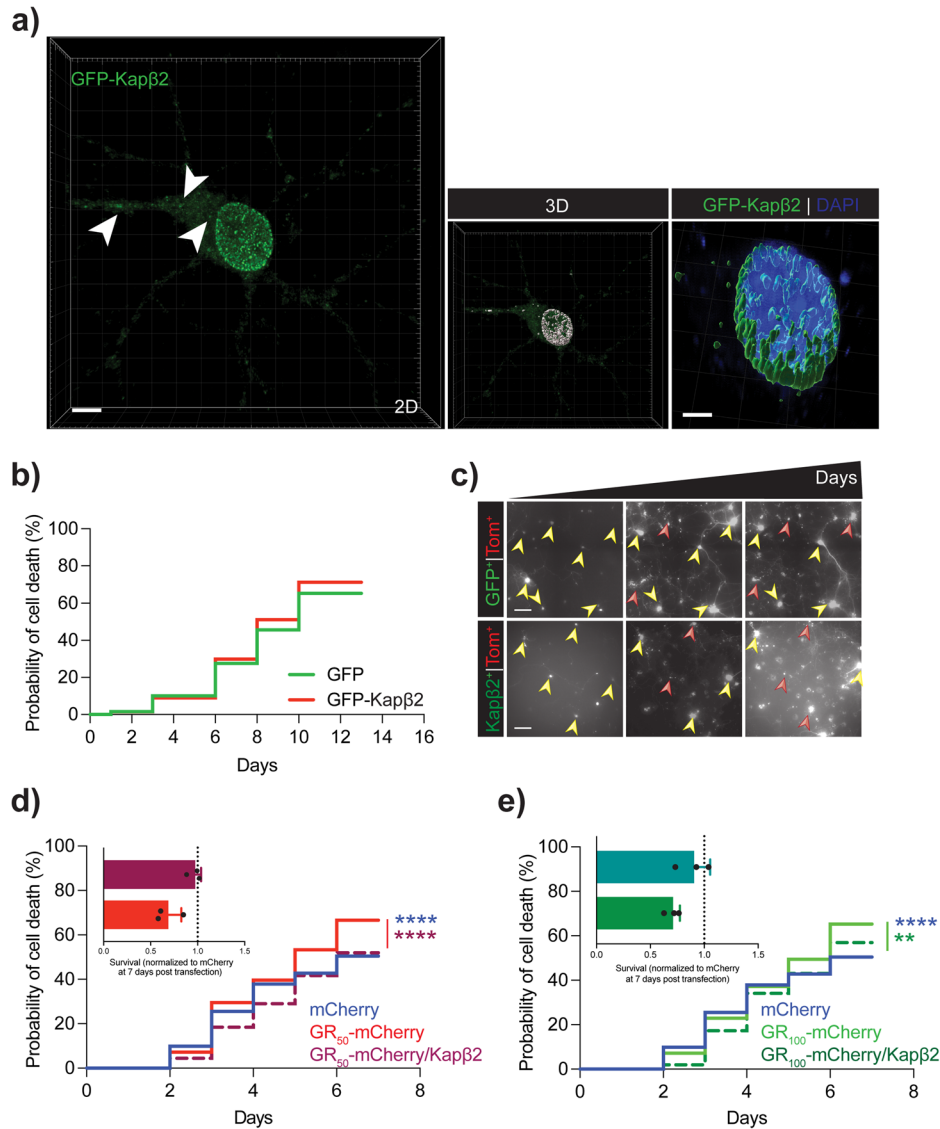


Fig. 4 | Increased expression of Kapβ2 does not affect neuronal viability. **a** Left: Confocal imaging of primary neurons transfected with GFP-Kapβ2. Arrows indicate cytoplasmic puncta. Green is GFP, and blue is DAPI. Scale bar = 5 μm. Center: Imaris 3D rendering of GFP-Kapβ2 expression in primary rat cortical neurons. Right: Magnification of Imaris' rendering of GFP-Kapβ2 puncta around the nucleus. Scale bar = 3 μm. **b** Probability of neuronal death via a cumulative risk of death plot of rat primary cortical neurons transfected with 200/400 ng of Tm⁺/GFP-Kapβ2⁺ (GFP used as control) per 150,000 cells. Neurons double positive Tm⁺/GFP⁺ were counted (n = 3 biological replicates, m > 150 neurons, Log-rank Mantel-Cox test: n.s. not significant). **c** Representative images of neurons over time transfected with 200/400 ng of Tm⁺/GFP⁺. Green is Kapβ2; red is Td-Tomato. Scale bar = 20 μm. **d** Probability of neuronal death via a cumulative risk of death plot of rat primary cortical neurons transfected with 400/400 ng of GFP-Kapβ2 (GFP alone used as control) and GR₅₀-mCherry (mCherry alone used as control) per 150,000 cells.

Neurons double positive GFP⁺/mCherry⁺ were counted (n = 3 biological replicates, m > 150 neurons, Log-rank Mantel-Cox test: mCherry vs GR₅₀-mCherry p < 0.0001; GR₅₀-mCherry vs GR₅₀-mCherry /GFP-Kapβ2 p < 0.0001). Inset: bar graph showing quantification of GR₅₀-mCherry and GR₅₀-mCherry /GFP-Kapβ2 overall survival normalized to mCherry 7 days post-transfection, n = 3 biological replicates. Data are represented as mean ± S.E.M. **e** Probability of neuronal death via a cumulative risk of death plot of rat primary cortical neurons transfected with 400/400 ng of GFP-Kapβ2⁺ (GFP alone used as control) and GR₁₀₀-mCherry (mCherry alone used as control) per 150,000 cells. Neurons double positive GFP⁺/mCherry⁺ were counted (n = 3 biological replicates, m > 150 neurons, Log-rank Mantel-Cox test: mCherry vs GR₁₀₀-mCherry p < 0.0001; GR₁₀₀-mCherry vs GR₁₀₀-mCherry /Kapβ2 p = 0.005). Inset: bar graph showing quantification of GR₁₀₀-mCherry and GR₁₀₀-mCherry /GFP-Kapβ2 overall survival normalized to mCherry at 7 days post-transfection, n = 3 biological replicates. Data are represented as mean ± S.E.M.

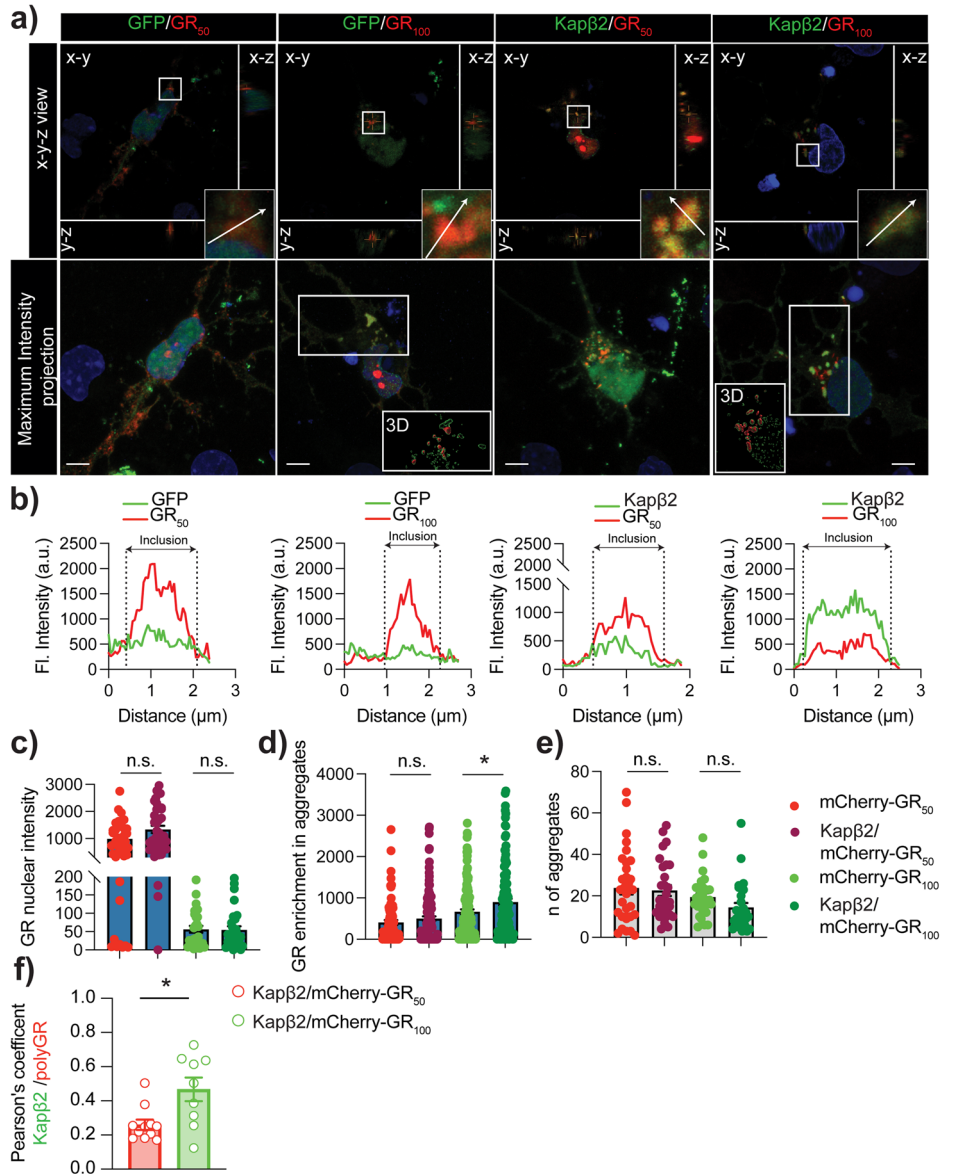
Discussion

Our study demonstrated the impact of modifying Kapβ2 levels on GR-mediated neuronal toxicity. We established that GR interacts with Kapβ2 in vitro in primary neuronal culture and in vivo in CNS tissues, such as the cortex and spinal cord of a GR-expressing transgenic knock-in mouse model. These studies were facilitated by the fusion of the GR protein to the GFP molecule, and thus, we have provided GFP-only controls for all the experiments to show the specificity of our findings for GR. Interaction studies in vivo are presented in this paper always using orthogonal methods aimed at making the claims more robust. For example, in animal tissues, the

co-IP data was analyzed by western blot, which supported the colocalization data analyzed by confocal microscopy. We didn't image the tissue of GFP-only mice using confocal microscopy due to the inefficient fluorescence signal of the GFP reporter^{6,14}.

Kapβ2 and GR have been implicated in the pathogenesis of certain forms of ALS and FTD. Kapβ2 is a nuclear import receptor that regulates the transport of substrate molecules critical for cell survival between the nucleus and the cytoplasm³⁵. Dysregulation of nuclear-cytoplasmic transport is thought to contribute to the pathogenesis of ALS and FTD, and it is possible that an interaction between Kapβ2 and GR could have implications for this

Fig. 5 | Increased expression of Kapβ2 mitigates GR neuronal toxicity. **a** Confocal analysis of neurons overexpressing GFP or Kapβ2 and GR₅₀-mCherry or GR₁₀₀-mCherry. The top row shows an x-y-z view, while the bottom row shows the maximum intensity projection of the Z plans acquired. Green is GFP, red is mCherry, and blue is DAPI. The white line represents the length over which GFP and mCherry fluorescence were analyzed. Scale bar = 10 μm. **b** Graph showing intensity profiles of GFP or mCherry fluorescence (a.u.) over distance (μm). **c** The bar graph shows quantification of GR₅₀-mCherry and GR₁₀₀-mCherry nuclear intensity. Data are represented as mean ± S.E.M. Only double positive cells were considered. (n = 3 biological replicates, m = at least 30 neurons/group, One-Way ANOVA, Tukey's multiple comparisons test, n.s. not significant). **d** The bar graph shows the quantification of GR₅₀-mCherry and GR₁₀₀-mCherry mean fluorescence intensity in GR-positive granules. Data are represented as mean ± S.E.M. Only double positive cells were considered. (n = 3 biological replicates, m = at least 30/group neurons, One-Way ANOVA, Tukey's multiple comparisons test, n.s. not significant). **e** The bar graph shows the quantification of the GR₅₀-mCherry and GR₁₀₀-mCherry aggregates per cell. Data are represented as mean ± S.E.M. Only double positive cells were considered. (n = 3 biological replicates, m = at least 30 neurons/group, One-Way ANOVA, Tukey's multiple comparisons test, n.s. not significant). **f** Pearson's coefficient analysis of GFP-Kapβ2 and GR₅₀-mCherry or GR₁₀₀-mCherry. Data are represented as mean ± S.E.M. (n = 3 biological replicates, m = 9–10 neurons/group, Student *t*-test, *P* < 0.05).



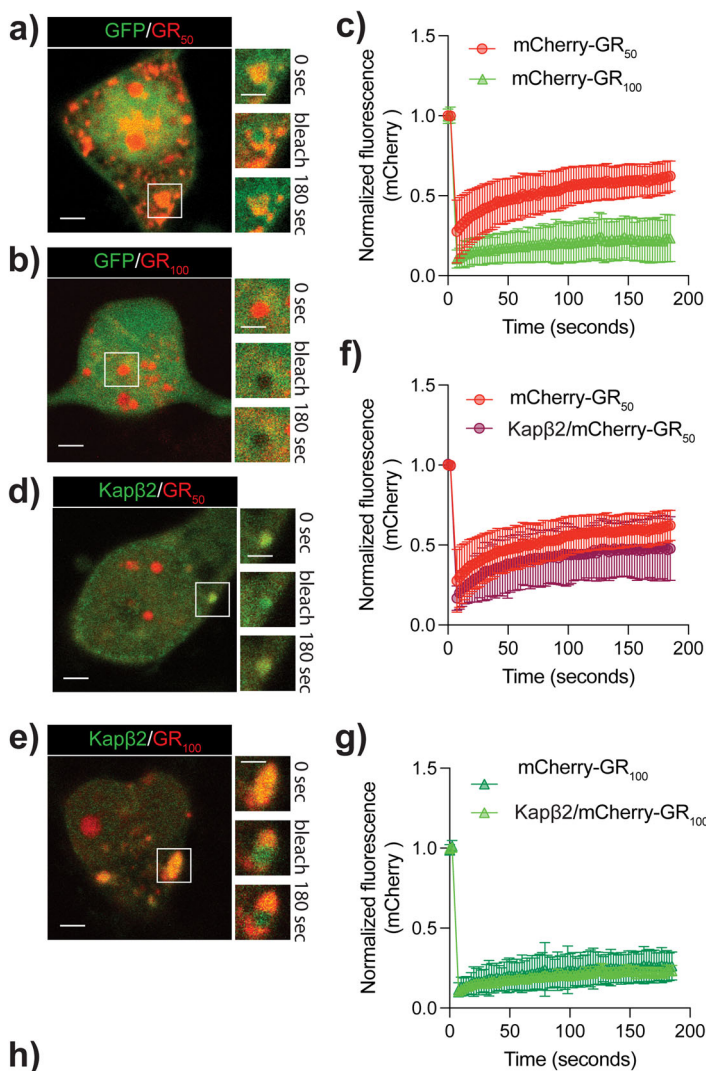
process. Indeed, we found that suppressing Kapβ2 levels elevates the risk of neuronal death. On the other hand, Kapβ2 overexpression shields neurons against GR-induced neurodegeneration.

The formation of GR aggregates is believed to be linked to several cellular dysfunctions in C9orf72-ALS/FTD, including impaired nucleocytoplasmic transport, altered proteostasis and RNA metabolism. Dysregulation of these cellular processes can lead to the accumulation of toxic protein inclusions, including GR aggregates, which can trigger a cascade of toxic events that lead to neuronal dysfunction and death. We demonstrated that Kapβ2 exhibits enrichment within GR aggregates but that its presence does not modify the mobile fraction of GR within the aggregates. To resolve protein aggregates, it's often necessary to increase their mobility. This allows other proteins, which are responsible for clearing the inclusion, to access the aggregates and extract the proteins that need to be degraded. This can facilitate the disassembly and degradation of the aggregates, freeing co-aggregated proteins essential for cell survival, such as TDP-43⁴⁵. We were thus not surprised to observe that Kapβ2 did not alter TDP-43 localization in the GR aggregates. TDP-43 mislocalization is a pathological feature of the majority of ALS cases. It refers to the abnormal accumulation or redistribution of TDP-43 in cytoplasmic inclusions in affected neurons and its depletion from the nucleus, where it physiologically resides⁴⁶. TDP-43 mislocalization triggers a cascade of toxic events that lead to neuronal

dysfunction and death^{47,48}. Hence, potential therapeutic strategies for ALS could be directed to prevent TDP-43 mislocalization and/or restore its nuclear localization. Several studies, including the present one, have also demonstrated a physical interaction between GR and TDP-43. For example, a study by ref. 10 showed that GR directly interacted with TDP-43 and sequestered it in cytoplasmic aggregates, leading to its depletion from the nucleus. This mislocalization of TDP-43 is thought to be a critical step in the pathogenesis of ALS and FTD.

In our in-vitro assay, we found that the addition of Kapβ2 hindered the entry of TDP-43 into the GR aggregates and allowed TDP-43 to remain soluble in the buffer. However, we failed to validate this mechanism in primary neurons in culture. Indeed, we did not observe an increase in nuclear TDP-43 re-localization. Interestingly, these results contradict the previous findings by Hutten et al., which showed that Kapβ2 could directly disrupt GR/TDP-43 co-aggregation, restoring TDP-43 nuclear localization. The ability of DPRs to disrupt the nucleo-cytoplasmic transport and indirectly promote TDP-43 aggregation was also shown by a recent study in HeLa cells^{18,49}. In our neuronal culture model, we observed co-aggregation of TDP-43 with GR₅₀ and GR₁₀₀ and a corresponding decrease in nuclear TDP-43. While Kapβ2 also localizes to the GR aggregates, it does not reduce TDP-43 localization in the aggregates or alter the TDP-43 nucleo/cytoplasmic ratio.

Fig. 6 | Kap β 2 does not change the dynamic properties of GR aggregates. **a** Representative images of the GR₅₀-mCherry bleached aggregates at the start (0 s), bleaching (5 s), and end (180 s). Scale bar = 10 μ m. **b** Representative images of the GR₁₀₀-mCherry bleached aggregates at the start (0 s), bleaching (5 s), and end (180 s). Scale bar = 10 μ m. **c** The graph shows fluorescence recovery over time for GR₅₀-mCherry and GR₁₀₀-mCherry. Data are represented as mean \pm S.E.M. (n = 3 biological replicates, m > 5 neurons, Student *t*-test, *P* < 0.001). **d** Representative images of the GFP-Kap β 2/GR₅₀-mCherry bleached aggregates at the start (0 s), bleaching (5 s), and end (180 s). Scale bar = 10 μ m. **e** Representative images of the GFP-Kap β 2/GR₁₀₀-mCherry bleached aggregates at the start (0 s), bleaching (5 s), and end (180 s). Scale bar = 10 μ m. **f** The graph shows fluorescence recovery over time for GR₅₀-mCherry and GFP-Kap β 2/GR₅₀-mCherry. Data are represented as mean \pm S.E.M. (n = 3 biological replicates, m > 5 neurons). **g** The graph shows fluorescence recovery over time for GR₁₀₀-mCherry and GFP-Kap β 2/GR₁₀₀-mCherry. Data are represented as mean \pm S.E.M. (n = 3 biological replicates, m > 5 neurons). **h** A table summarizing mean and S.E.M. of the mobile fraction, t1/2 (τ), and the significance level for the FRAP curve profiles presented in (f) and (g); n.s. not significant.



	Mobile Fraction		T half (τ)		Significance levels
	Mean	SEM	Mean	SEM	
mCherry-GR50	0.5561	0.06455	54.83	12.51	n.s.
mCherryGR50-Kapbeta2	0.4705	0.06063	38.4	10.05	
mCherry-GR100	0.2895	0.0724	61.2	15.62	n.s.
mCherryGR100-Kapbeta2	0.416	0.08978	72.52	16.46	

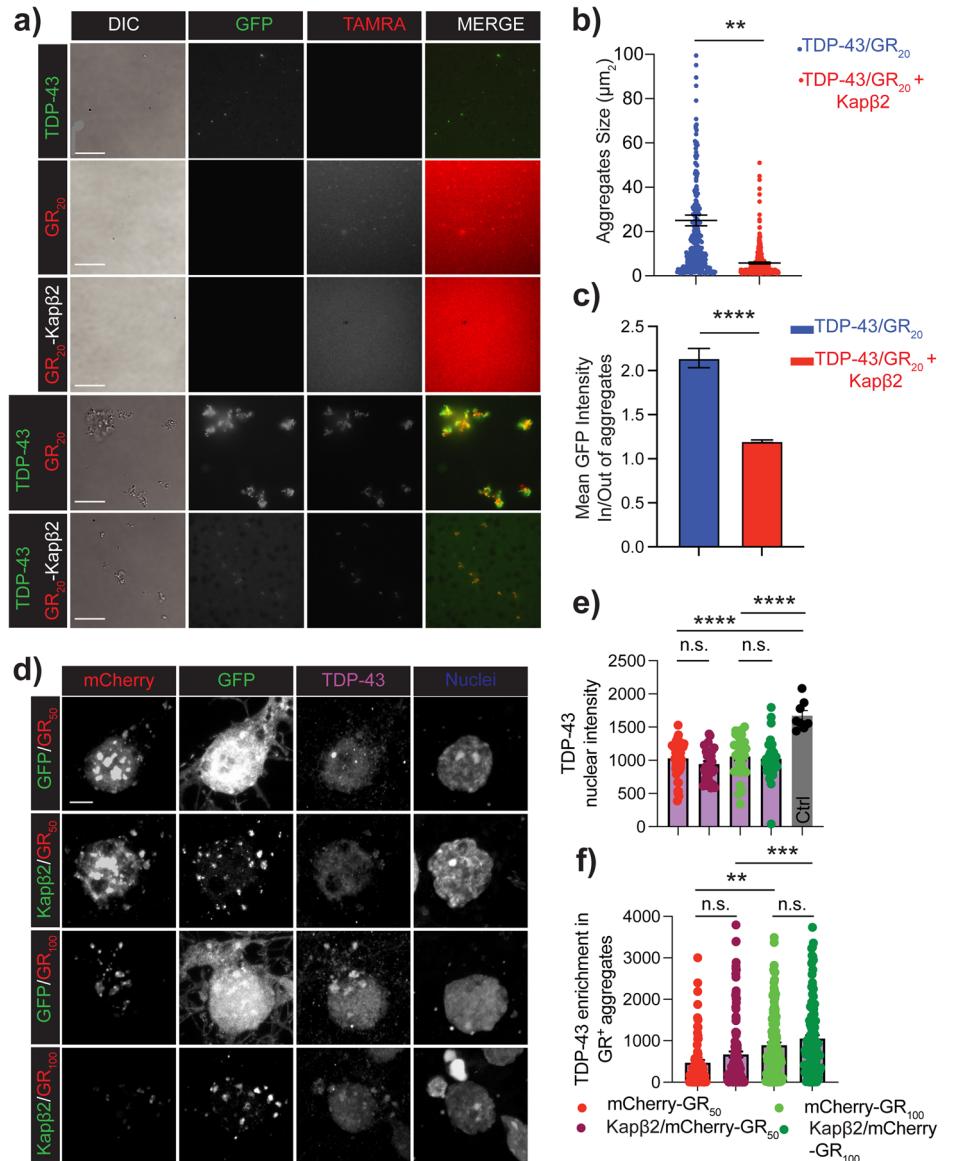
Numerous studies in the ALS/FTD field have focused on the disruption of the nuclear pore complex and the nuclear import/export activity^{7,50,51}. Defects in the proper import/export of critical proteins are associated with DPRs or G₄C₂ repeat-containing C9orf72 RNA transcripts. At the same time, TDP-43 aggregates trigger defects in nucleo-cytoplasmic transport, highlighting the importance of these pathways in disease^{16,52}. Therefore, conducting studies that further characterize these pathways is crucial. A recent study sheds light on the potential consequences of R-rich DPR interaction with the nuclear import receptors (NIRs), proteins responsible for transporting molecules inside the cell nucleus through the nuclear pore complex⁵³. The study revealed that NIR recruitment into DPR aggregates impairs their ability to maintain the solubility of other RNA-binding proteins (RBPs), such as FUS. Even though it is outside the scope of this study to analyze the behavior of the different RBPs, in the case of TDP-43, we did not observe TDP-43 aggregates other than the ones formed by co-aggregation with GR and Kap β 2.

The pathogenesis of C9orf72-associated ALS/FTD is likely multifactorial, involving multiple mechanisms that interact with each other. A

Kap β 2-based therapeutic strategy might not bring enough benefits as a stand-alone treatment for ALS but might work in conjunction with drugs targeting different pathways. Kap β 2 levels could be raised in neurons using a gene therapy approach such as mRNA-nanoparticle technology⁵⁴. Future studies would also be directed to screening for compounds that can induce the expression of Kap β 2 in neurons. Another intriguing therapeutic possibility is *via* promoting arginine methylation. For instance, the Kap β 2-FUS interaction is modulated by the FUS methylation status⁵⁵. Arginine methylation is also a GR post-translational modification that sometimes dictates disease severity⁵⁶. The most abundant GR methylation status in post-mortem tissues is the asymmetric di-methylated form, but GR can be present with symmetrical di-methylation or mono-methylation. It would be essential to expand on this concept and study how the different methylation status/conditions of GR influence Kap β 2 binding and, thus, GR toxicity. These studies could entail evaluating the ideal dosage and delivery modes of Kap β 2 and any possible adverse reactions and enduring impacts on the brain.

Some intrinsic limitations in our study should be taken into consideration when interpreting our results. We recognize that Pearson's

Fig. 7 | Increasing Kapβ2 expression levels does not affect TDP-43 subcellular localization in the presence of GR. **a** Epifluorescence images of condensate formation in vitro in a test tube containing equimolar concentration (5 μM) of TDP-43, GR₂₀, and Kapβ2. Green is TDP-43, and red is GR₂₀. Scale bar = 15 μm. **b** Quantification of the size of TDP-43/GR₂₀ aggregates in the presence or absence of Kapβ2. Data are represented as mean ± S.E.M. (n = 3 biological replicates, Student *t*-test, *P* < 0.01). **c** Ratio between the mean GFP intensity inside and outside TDP-43/GR₂₀ aggregates in the presence or absence of Kapβ2. Data are represented as mean ± S.E.M. (n = 3 biological replicates, Student *t*-test, *P* < 0.0001). **d** Confocal analysis of neurons over-expressing GFP or Kapβ2 and GR₅₀-mCherry (top row) or GR₁₀₀-mCherry (bottom row). Scale bar = 5 μm. **e** Single-nuclei TDP-43 staining quantification. Data are represented as mean ± S.E.M. Only double positive cells were considered. (n = 3 biological replicates, m = at least 9 neurons/group, Student *t*-test, *P* < 0.01; *P* < 0.001). **f** TDP-43 quantification into GR aggregates. Data are represented as mean ± S.E.M. Only double positive cells were considered. (n = 3 biological replicates, m = at least 30 neurons/group, Student *t*-test, *P* < 0.01; *P* < 0.001).



coefficient colocalization scores do not entirely demonstrate physical interaction between proteins, which is why we sought to prove the GR-Kapβ2 interaction with additional techniques, such as co-IP studies. We recognize that the presence of the GFP reporter moiety fused to the GR polypeptide could interfere with some of the experiments conducted; for example, in co-IP experiments we reported binding of Kapβ2 to the GFP reporter moiety that we expressed in neurons as control. Therefore, we sought to further prove the GR-Kapβ2 interaction by rigorously quantifying the co-IP results and running and quantifying reverse co-IP using Kapβ2 antibodies. Overall, we believe that using established, orthogonal biochemical and imaging techniques is highly effective in demonstrating the interaction between GR and Kapβ2 in primary neurons and CNS tissue.

Methods

Human tissues

Human post-mortem CNS tissue from healthy controls and patients carrying the C9ORF72 intronic nucleotide repeat expansion was obtained from the Target ALS and the Weinberg ALS center biobank. Information and demographics of patients and controls are presented in Supplementary Table 4. Human post-mortem tissues (fresh frozen) were stored at -80 °C.

Cell cultures

HEK293 cells were cultured in DMEM medium (Cytiva Cat.# SH30243.LS) supplemented with 10% FBS (Cytiva Cat.# SH30071.01HI), penicillin, and streptomycin (Thermo Fisher Scientific Cat.# SV30010). Cells were passaged every 3–4 days using 0.05% trypsin (Corning Cat.# 25-051-C).

Primary cortical neurons

After meninges removal, brains were dissected from embryonic day 16 (E16) rat embryos. Cortices and midbrain regions were cut into small pieces and incubated on a shaker at 80 rcf for 45 min at 37 °C in 0.2% trypsin in HBSS without Ca²⁺ and Mg²⁺ (Cytiva Cat.# SH30588.01). FBS (Cytiva Cat.# SH30071.01HI) was added, and the cell suspension was centrifuged at 800 rcf for 10 min. at 4 °C. Cells were washed with Ca²⁺ and Mg²⁺ free HBSS and centrifuged at 800 rcf for 10 min. at 4 °C. The cell suspension was then passed through a 70 μm strainer (Foxy Life Sciences Cat.# 410-0002-OEM) to remove undigested connective tissue and large cell clumps. Dispersed cells were then counted and plated in poly-D lysine-coated plates. The following plating densities were used: 150,000 cells/well in 24 well plates, 300,000 cells/well in 12 well plates, and 5,000,000 cells/dish in 10 cm dishes. Arsenite 0.5 mM was applied for 30 min. immediately before processing the neurons for analysis. DSP (dithiobis(succinimidyl propionate)) was added

to the neurons before harvesting at a concentration of 0.1 mM to the neurons in culture before processing them for western blot analysis.

Animals

B6.C-Tg(CMV-cre)1Cgn/J::B6.C-GR50 (GR₅₀) or B6.C-Tg(CMV-cre)1Cgn/J::B6.C-GFP (GFP) mice were generated as described in ref. 6. At 12 months, male mice were sacrificed, and cortices and spinal cords were collected and frozen in liquid N₂ or embedded in OCT. Frozen samples were stored at -80 °C till the time of processing. All animal procedures were compliant with the ARRIVE guidelines and approved by IACUC. We have complied with all relevant ethical regulations for animal use.

Plasmids and siRNA

The following plasmids were used: pCDNA3_hSyn_Td_Tomato; pCDNA3_hU6_Flag_mCherry; pCDNA3_hU6_Flag_GR₅₀_mCherry; pCDNA3_hU6_Flag_GR₁₀₀_mCherry; pCDNA3_CMV_eGFP; pCDNA3_CMV_eGFP_Kapβ2.

eGFP and eGFP_Kapβ2 were co-transfected with Td_Tomato at a DNA concentration ratio of 1:2 (200 ng/400 ng) or 1:4 (200 ng/800 ng). eGFP and eGFP_Kapβ2 were co-transfected with mCherry, mCherry_GR₅₀ and mCherry_GR₁₀₀ at 1:1 ratio (400 ng/400 ng).

Human TDP-43 and TDP-43-GFP were subcloned into pE-SUMO (LifeSensors, Malvern, PA). All plasmid inserts were sequenced and confirmed to be correct.

To silence Kapβ2, 50 μM of ON-TARGETplus siRNA-TNPO1-Smart Pool (Horizon Discovery, L-086861-02-0005) was used. 50 μM of AllStars Negative Control scramble siRNA (Qiagen Cat. #1027280) was used as control.

Transfection

Lipofectamine 2000 (Fisher Scientific Cat. #11-668-019) was used to transfect HEK cells and cortical neurons (1 μL Lipo2000/500 ng total D.N.A.). HiPerfect Transfection Reagent (Qiagen Cat. #301705) was used to transfect siRNA (8 μL HiPerfect/50 nM siRNA). siRNA was transfected 24 h before plasmids transfection. For cortical neurons, Lipo/DNA or RNA mix was incubated with the neurons for 1 h, and then cell media were changed with fresh ones. For HEK293 cells, the mixture was incubated with the cells overnight.

Lentivirus constructs production

HEK293 cells were transfected with the following plasmids: pLenti_hSyn_Flag_GR₅₀_eGFP, psPAX2 (Addgene Plasmid #12260), pMD2.G (Addgene Plasmid #12259). Plasmids were diluted in DMEM, and PEI MAX was added as a transfection reagent. The mix was incubated with HEK293 cells confluent at 70% for 5 h; the media was changed with a fresh one. Cells supernatant was collected 48 h after transfection and centrifuged for 10 min at 2000 rcf at 4 °C. Lentivirus Concentrator (OriGene Technologies Cat. #TR30025) was added to the supernatant and incubated overnight at 4 °C. To pellet the virus, the media was centrifuged at 500 rcf for 45 min at 4 °C. Viral particles were then resuspended in Ca²⁺ and Mg²⁺ free PBS (Cytiva Cat. #SH30028. L.S.), aliquoted and immediately frozen in liquid N₂.

Purification of recombinant proteins

His₆-SUMO1 N-terminally tagged TDP-43-WT and TDP-43-GFP were purified as described (McGurk et al., 2018) and overexpressed in BL21(DE3) RIL *E.coli* cells. These cells were then sonicated on ice in 50 mM HEPES (pH 7.5), 2% TritonX-100, 300 mM NaCl, 30 mM imidazole, 5% glycerol, 2 mM β-mercaptoethanol, and protease inhibitors (cOmplete, EDTA-free, Roche). The recombinant TDP-43 proteins were purified over Ni-NTA agarose beads (Qiagen) and eluted using 50 mM HEPES (pH 7.5), 150 mM NaCl, 300 mM imidazole, 5% glycerol, and 5 mM DTT. The buffer was exchanged with the same buffer without imidazole. The eluate containing the recombinant TDP-43 proteins was then frozen in liquid N₂ and stored as aliquots at -80 °C until use.

Kapβ2 was purified as described (ref. 34). In brief, *E. coli* BL21-CodonPlus(DE3)-RIL cells (Agilent) were transformed with GST-Tev-Kapβ2 plasmid, and expression was induced overnight at 25 °C with 1 mM IPTG. Cells were pelleted and resuspended in Tris buffer (50 mM Tris pH 7.5, 100 mM NaCl, 1 mM EDTA, 20% (v/v) glycerol, 2 mM DTT, supplemented with protease inhibitors), then lysed by sonication. Cell lysate was then loaded onto glutathione Sepharose™ 4 Fast Flow resin (GE Healthcare) and washed with Tris buffer, followed by ATP buffer (50 mM Tris pH 7.5, 100 mM NaCl, 1 mM EGTA, 0.5 mM MgCl₂, 5 mM ATP, 20% glycerol, 2 mM DTT, supplemented with protease inhibitors), then washed and eluted with Buffer A (20 mM imidazole, 75 mM NaCl, 1 mM EDTA, 20% (v/v) glycerol, 2 mM DTT). Finally, the protein was cleaved with Tev protease and purified on a HiTrap Q HP column (GE Healthcare) using a salt gradient. Purified protein was concentrated, flash frozen, and stored at -80 °C. Before the aggregation assay, the protein was thawed and centrifuged at 16,100 × g for 10 min to remove any preformed aggregates. Protein concentration was determined by Bradford assay (Bio-Rad, Hercules, CA).

Equimolar concentrations of Kapβ2, TDP-43, and GR₂₀ (5 μM) were used. 200 nM His₆-SUMO-TDP-43-GFP and 100 nM TAMRA-GR₂₀ were added to visualize TDP-43 and GR₂₀.

Peptides

Chemically synthesized GR₂₀ and Tetramethylrhodamine (TAMRA)-tagged GR₂₀ were obtained as a lyophilized powder from Peptide2.0 and dissolved in PBS.

Sample preparation

100 mg of fresh frozen lumbar spinal cord samples were homogenized in 1% SDS using a 15 ml Dounce Homogenizer. The homogenate was centrifuged at 3000 rcf for 20 min at 4 °C to remove tissue debris. Protein estimation was performed on the clear homogenate using a BCA assay (Pierce BCA kit #23225). 30 μg of protein samples are loaded for Western blot analysis.

For mouse tissues: 50 mg of CNS tissues were chopped into small pieces, incubated in RIPA for 2 h, and homogenized by pipetting every 20/25 min. Samples were then sonicated using Bioruptor Pico-Diagenode.

For cell cultures: Cells were harvested in PBS and centrifuged at 500 rcf for 3 min. PBS was removed by suction, and samples were resuspended in 80 μL of RIPA with protease inhibitor (Sigma-Aldrich Cat# P2714-1BTL). Cells were incubated for 15 min at 4 °C on an orbital shaker and then sonicated. After sonication, samples were centrifuged at 16,000 rcf for 5 min at 4 °C. Supernatant was kept, and BCA was used to measure the protein content of each sample.

Western blot

Cell cultures and animal tissues: 15 μg of protein extracts were loaded on pre-cast Stain Free gels (Bio-Rad Cat.#4568034) and run for 1 h at 100 V. Gels were then transferred on PVDF membrane (Millipore Cat.#IPVH00010) overnight at 4 °C at 30 V and developed with primary and secondary antibodies at the indicated concentration. Before transfer, gels were cross-linked by UV light exposure for 5 min, and total protein content was then revealed on the membrane by UV light exposure. Membranes were developed with SuperSignal™ West Femto Maximum Sensitivity Substrate (Thermo Fisher Scientific Cat#34094) and imaged using ChemiDOC XRS+ System (Bio-Rad).

Human samples: The gels were U.V. activated for 5 min before transferring onto the 0.22 μm nitrocellulose membrane. The semi-dry transfer was done using a Trans-Blot Turbo Transfer System (Bio-Rad) at 25 mV for 10 min. After the transfer, a stain-free blot image was captured and used as total protein content. The blot was processed as previously described. The quantification was done using Image Lab Software (Bio-Rad); the intensity of the Kapβ2-positive band is normalized to its total proteins. Quantification was performed using Image Lab software. Adjusted volume was measured for each band and divided by the adjusted volume calculated, considering the entire lane of total proteins. The abundance of

the protein of interest was normalized to the total amount of proteins in each lane, therefore removing variations associated with comparing abundance to a single protein arbitrarily chosen as housekeeping protein (e.g., GAPDH). Total protein normalization is more compatible with detecting and quantifying proteins of lower abundance.

Immunoprecipitation

Flag: Immunoprecipitation was carried out using anti-Flag agarose beads (mouse IgG agarose beads were used as control). Rat primary cortical neurons and tissues were extracted in IP buffer containing 50 mM Tris-HCl (pH 7.5), 150 mM NaCl, 1 mM EDTA, 0.5% NP-40, 100 mM EDTA (pH 8.0) supplemented with protease inhibitor (Sigma-Aldrich Cat.# P2714-1BTL). After incubating at 4°C for 30 min., the samples were sonicated and then centrifuged for 10 min. at 10,000 rcf. Bradford assay was used to determine protein concentration. The agarose beads were added to 600 µg of cell lysates and incubated at 4°C for 24 h under constant shaking. Cell lysates were centrifuged for 1 min. at 1000 rcf to collect the supernatant. The pellets were washed five times, but only the first wash was collected. After the last centrifugation, the samples were eluted with SDS-PAGE loading dye at 95°C for 5 min. The entire eluate was run for Western blot. 2% of total lysate was used as input.

GFP and Kapβ2: Following manufacturer instructions, immunoprecipitation was carried out using magnetic beads (Thermo Fisher Scientific Cat.# 88804). Briefly, 25 µL of magnetic beads were conjugated with 10 µg of the desired antibody overnight and then crosslinked for 30 min using DSS (disuccinimidyl suberate). The obtained beads-antibody complex was incubated with cell or tissue lysates overnight. The next day, beads were washed, and the bound protein was eluted. The entire eluate was run for Western blot. 2% of total lysate was used as input. For Kapβ2 IP, a double volume of beads was used.

Quantification: signal specifically corresponding to Kapβ2 and GFP bands was measured with ImageLab and the ratio was calculated between the respective adjusted volumes.

Immunofluorescence

Primary cortical neurons were fixed for 20 min at 37°C with 4% PFA and incubated in PermBlock solution (2% BSA, 0.3% Triton-x, 5% donkey serum in PBS). Primary antibodies were diluted in 0.1% BSA cells and were incubated overnight at 4°C on an orbital shaker. The following day, cells were washed two times with PBS at room temperature for 10 min and incubated with the appropriate secondary antibody for 1 h at room temperature. Cells were washed twice in PBS and incubated with Hoechst solution (Thermo Fisher Scientific Cat.# 62249) for 10 min at room temperature to stain the nuclei. After a final rinse in PBS, coverslips were mounted on glass slides using AquaMount (Lerner Laboratories Cat.# 13800).

Tissues were cryo-sectioned using Cryostar NX50. 20 µm thick sections were placed on glass slides and incubated for 10 min in 4% PFA. Slides were then washed in TBS-T for 10 min and incubated for 1 h at room temperature in PermBlock solution (2% BSA, 0.3% Triton-x, 5% donkey serum in PBS) and then incubated with primary antibody diluted in 1% BSA, 0.3% Triton-x and 1% donkey serum overnight at 4°C in a humidified chamber. The following day, slides were washed with TBS-T, incubated with the appropriate fluorescent secondary antibody for 1 h at room temperature, rinsed twice in TBS-T, incubated for 10 min with Hoechst (Thermo Fisher Scientific Cat.# 62249), and mounted on coverslips using AquaMount (Lerner Laboratories Cat.# 13800) for imaging analysis.

Antibodies and dilutions

Primary antibodies: anti-Kapβ2 (RRID:AB_2206884, Santa Cruz Biotechnology, Inc Cat.# sc-101539; WB dilution 1:1000); anti-Kapβ2 (RRID:AB_262123, Sigma Cat.# T0825; IF dilution 1:500); anti-Map2 (RRID:AB_2138178 Novus Cat.#NB300-213; IF dilution 1:2000); anti-GFP (RRID:AB_11042881, Proteintech Cat.#50430-2-AP, WB dilution 1:1000); anti-TDP-43 (RRID:AB_615042, Proteintech Cat.#10782-2-AP; IF dilution

1:500); anti-GAPDH (RRID:AB_2107436, Proteintech Cat.#60004-1-Ig; WB dilution 1:1000); Neun (D4G40) XP (RRID:AB_2651140, Cell Signaling Technology Cat.#24307; IF dilution 1:500); FUS (RRID:AB_2247082, Proteintech Cat.#11570-1-AP; IF:1:500).

Secondary HRP-conjugated antibodies: HRP-Conjugated anti-rabbit (RRID:AB_772191, Cytiva Cat.# NA9340-1ML; WB dilution 1:10,000); HRP-Conjugated anti-mouse (RRID:AB_772193, Cytiva Cat.# NA9310-1ML; WB dilution 1:10,000); HRP-Conjugated anti-rat (RRID:AB_2936877, Sigma Cat.# AP136P; WB dilution 1:3,000);

Secondary fluorescent antibodies: AlexaFluor-546 anti-mouse (RRID:AB_2534012, Thermo Fisher Scientific Cat.# A10036; IF dilution 1:1,000); AlexaFluor-647 anti-rabbit (RRID:AB_2536183, Thermo Fisher Scientific Cat.# A31573; IF dilution 1:1,000); AlexaFluor-647 anti-chicken (RRID:AB_2762845, Thermo Fisher Scientific Cat.# A32933; IF dilution 1:1,000);

Extraction of total RNA and quantitative Real-Time PCR

Total RNA was extracted using Trizol Reagent (Ambion Cat.# 15596026) following the manufacturer's instructions. Briefly, cells were lysed in Trizol Reagent and homogenized using a syringe for insulin. RNA was then extracted in isopropanol. Samples were centrifuged for 15 min. at 12,000 rcf. The RNA-containing pellet was washed with 75% ethanol and centrifuged for 5 min. at 7500 rcf. Dried pellets were resuspended in DEPC water, and concentration was assessed with Nanodrop. 500 ng of total RNA was first treated with DNase I (Thermo Fisher Scientific Cat.# EN0521) and retro-transcribed using SuperScript™ IV Reverse Transcriptase (Thermo Fisher Scientific Cat.# 18090010). The cDNA was diluted 1:2 and used for qRT-PCR, which was performed using the following TaqMan assay: GAPDH-VIC (Thermo Fisher Scientific Cat.# 4352338E) and Kapβ2-FAM (Thermo Fisher Scientific Cat.# 4331182 Assay# Rn01489969_m1). 50 ng of cDNA was used per reaction. Samples were analyzed using the Design and Analysis tool by Thermo Fisher Scientific. Results are shown as fold change using the $2^{-\Delta\Delta Ct}$ method.

Confocal imaging analysis

Confocal images were taken on a Nikon A1R confocal microscope with a 60X objective. Z-stacks were taken for each image. 0.2 µm Z-stacks were taken to perform colocalization studies and puncta counting using a built-in function in Imaris. 1 µm stacks were taken for TDP-43 nuclear intensity studies. Maximum intensity projection was then generated through a built-in function of the A1R analysis software. The nuclei of each co-transfected cell were selected as the region of interest, and TDP-43 intensity was assessed. The mask was made on the mCherry channel to analyze aggregate content, and the TDP-43 fluorescence was subsequently evaluated. For Kapβ2 nuclear and cytoplasmic quantification maximum intensity projections were generated, and ROI were drawn around nucleus and cytoplasm and intensity referred to the Kapβ2 channel was measured. The ratio between nuclear and cytoplasmic intensities in the same cell was then calculated.

FRAP experiment was performed in green (GFP or GFP-Kap2) and red (mCherry, GR50-mCherry, GR100-mCherry) fluorescent cells. Aggregates were selected as regions of interest and photobleached for 2 s. with blue light with laser power at 25% power. Following photobleaching, images were taken every 2 s for 3 min and analyzed with Nikon A1R software. Normalization and curve fitting were performed using the online tool EasyFRAP (normalization was performed using double normalization, and curve fitting was performed using double equation). The fluorescence recovery intensity curves were represented over time using Prism GraphPad 9.0. The mobile fraction in FRAP experiments represents the proportion of molecules or particles that can freely move within the sample after photobleaching. The mobile fraction was calculated using the following formula: Mobile Fraction = Mobile Fluorescence Recovery / Initial Fluorescence Loss where the mobile fluorescence recovery is the increase in fluorescence signal after photobleaching, indicating the recovery of mobile molecules, and the initial fluorescence loss is the initial decrease in fluorescence signal due to photobleaching.

Time-lapse microscopy

Cells were imaged every 2 days after transfection. 20× objective was used, and 25 fields/wells were acquired. Only cells positives for both Kap β 2 and mCherry were counted. Cells were scored dead when they disappeared from the field of view or clear signs of neurite fragmentation appeared. Kaplan Meier curves were then constructed in Prism GraphPad 9.0.

Visualization of TDP-43 Condensates

His₆-SUMO1-TDP-43 (5 μ M) was incubated with an equimolar concentration of (GR)₂₀ for 1 h at room temperature in PBS. 200 nM His₆-SUMO1-TDP-43-GFP and 100 nM TAMRA-(GR)₂₀ were added to visualize TDP-43 and (GR)₂₀. The reaction mixture was incubated at room temperature for 1 h, and samples were spotted onto a coverslip and imaged by DIC and fluorescent microscopy using a Leica DMi8 Inverted microscope. To inhibit condensation, 5 μ M Kap β 2 was added at the beginning of the assay.

Proteomics analysis

Publicly available data sets from ref. 44. were downloaded from massive.ucsd.edu (MassIVE MSV000088581). Analysis and statistical comparison of protein abundance were performed using basic packages (ggplot, ggplot2) of R (version 4.0.5) and Rstudio (version 2022.07.2).

Transcriptomics analysis

In this study, we performed a transcriptomic analysis using publicly available datasets to investigate Kap β 2 expression patterns in iPS-derived cortical neurons and ALS patients' cerebral tissue.

For the Answer ALS data: The raw sequencing data were processed using quality control metrics and aligned to a reference genome using Kallisto. Differential gene expression analysis was performed using DESeq2. Kap β 2 expression levels across samples were analyzed with ggplot2, and statistical analysis was carried out using GGPUBR.

For the human tissue data, raw counts were downloaded from https://github.com/NathanSkene/ALS_Human_EWCE. Kap β 2 expression levels across samples were analyzed with ggplot2; statistical analysis was done using GGPUBR.

Statistics and reproducibility

All experiments were performed at least 3 times ($n \geq 3$). At least three mice/group were used. For live-cell imaging, >150 neurons/condition were counted for each n . For colocalization, puncta counting, and TDP-43 intensity, ≥ 10 neurons/condition were counted for each n . For the FRAP experiment, ≥ 5 cells/conditions were analyzed for each n . When two groups were compared, the Kolmogorov-Smirnov test assessed the normality of each population. If the two populations' results were normally distributed, then the unpaired t-student test was performed using the built-in function in Prism GraphPad 9.0. If one or both populations were not normally distributed, then the Mann-Whitney test was used to compare ranks or the Kolmogorov-Smirnov test was used using Prism GraphPad 9.0. The log-rank and Cox proportional hazards tests compared the Kaplan Meier curves and the statistical significance between curves was assessed with Cox (GraphPad software). For the FRAP experiment, statistical differences between the curves were evaluated by curve analysis (one-way ANOVA test) in Prism GraphPad 9.0.

Reporting summary

Further information on research design is available in the Nature Portfolio Reporting Summary linked to this article.

Data availability

The data that support the findings are available at the following <https://doi.org/10.5061/dryad.v41ns1s4f>. All uncropped blots are presented in Supplementary Fig. 8. Deposited Data from Liu et al., MSV000088581. Deposited Data from Manberg et al., https://raw.githubusercontent.com/NathanSkene/ALS_Human_EWCE/master/Data/Raw/GSE67196_Petrucci2015_ALS_genes.rawcount_EXP.csv. Deposited Data for analysis

of iPS derived cortical neurons come from the Answer ALS repository <https://dataportal.answersals.org/home>. All the data are available from the corresponding author upon request.

Code availability

Custom codes were used to analyze transcriptomics data from public repositories using R studio. These codes are available at the following <https://doi.org/10.5061/dryad.v41ns1s4f>.

Received: 19 July 2023; Accepted: 19 March 2024;

Published online: 28 March 2024

References

- Dejesus-hernandez, M. et al. Expanded GGGGCC hexanucleotide repeat in non-coding region of C9ORF72 causes chromosome 9p-linked frontotemporal dementia and amyotrophic lateral sclerosis. *Neuron* **72**, 245–256 (2011).
- Renton, A. E. et al. A hexanucleotide repeat expansion in C9ORF72 is the cause of chromosome 9p21-linked ALS-FTD. *Neuron* **72**, 257–268 (2011).
- Feldman, E. L. et al. Amyotrophic lateral sclerosis. *Lancet* **400**, 1363–1380 (2022).
- Gendron, T. F. & Petrucelli, L. Disease mechanisms of C9ORF72 repeat expansions. *Cold Spring Harb. Perspect. Med.* **8**, 1–22 (2017).
- Wen, X. et al. Antisense proline-arginine RAN dipeptides linked to C9ORF72-ALS/FTD form toxic nuclear aggregates that initiate invitro and invivo neuronal death. *Neuron* **84**, 1213–1225 (2014).
- Verdone, B. M. et al. A mouse model with widespread expression of the C9orf72-linked glycine-arginine dipeptide displays non-lethal ALS/FTD-like phenotypes. *Sci Rep.* **12**, 5644 (2022).
- Coyne, A. N. et al. G4C2 Repeat RNA Initiates a POM121-Mediated Reduction in Specific Nucleoporins in C9orf72 ALS/FTD. *Neuron* **107**, 1124–1140.e1111 (2020).
- Moens, T. G. et al. C9orf72 arginine-rich dipeptide proteins interact with ribosomal proteins in vivo to induce a toxic translational arrest that is rescued by eIF1A. *Acta Neuropathol.* **137**, 487–500 (2019).
- Maor-Nof, M. et al. p53 is a central regulator driving neurodegeneration caused by C9orf72 poly(PR). *Cell* **184**, 689–708.e620 (2021).
- Chew, J. et al. Aberrant deposition of stress granule-resident proteins linked to C9orf72—associated TDP-43 proteinopathy. *Mol. Neurodegener.* **14**, 1–15 (2019).
- Boeynaems, S. et al. Phase separation of C9orf72 dipeptide repeats perturbs stress granule dynamics. *Mol. Cell* **65**, 1044–1055.e1045 (2017).
- Cook, C. N. et al. C9orf72 poly(GR) aggregation induces TDP-43 proteinopathy. *Sci. Transl. Med.* **12**, 1–12 (2020).
- Choi, S. et al. C9ORF72-ALS/FTD-associated poly(GR) binds ATP5 alpha1 and compromises mitochondria function in vivo. *Nat. Neurosci.* **22**, 851–862 (2019).
- Gleixner, A. M. et al. NUP62 localizes to ALS/FTLD pathological assemblies and contributes to TDP-43 insolubility. *Nat. Commun.* **13**, 3380 (2022).
- Vanneste, J. et al. C9orf72-generated poly-GR and poly-PR do not directly interfere with nucleocytoplasmic transport. *Sci. Rep.* **9**, 1–10 (2019).
- Hayes, L. R., Duan, L., Bowen, K., Kalab, P. & Rothstein, J. D. C9orf72 arginine-rich dipeptide repeat proteins disrupt karyopherin-mediated nuclear import. *eLife* **9**, 1–29 (2020).
- Hutten, S. et al. Nuclear import receptors directly bind to arginine-rich dipeptide repeat proteins and suppress their pathological interactions. *Cell Rep.* **33**, 108538 (2020).
- Khosravi, B. et al. Cytoplasmic poly-GA aggregates impair nuclear import of TDP-43 in C9orf72 ALS/FTLD. *Hum. Mol. Genet.* **26**, 790–800 (2017).

19. Lee, K.-H. et al. C9orf72 dipeptide repeats impair the assembly, dynamics, and function of membrane-less organelles. *Cell* **167**, 774–788.e717 (2016).
20. Kwon, I. et al. Poly-dipeptides encoded by the C9ORF72 repeats bind nucleoli, impede RNA biogenesis, and kill cells I/min. *Science* **345**, 1139–1145 (2015).
21. Stewart, M. Molecular mechanism of the nuclear protein import cycle. *Nat. Rev. Mol. Cell Biol.* **8**, 195–208 (2007).
22. Izaurralde, E., Kutay, U., von Kobbe, C., Mattaj, I. W. & Gorlich, D. The asymmetric distribution of the constituents of the Ran system is essential for transport into and out of the nucleus. *EMBO J.* **16**, 6535–6547 (1997).
23. Dasso, M. The Ran GTPase: theme and variations. *Curr. Biol.* **12**, R502–R508 (2002).
24. Rout, M. P., Aitchison, J. D., Magnasco, M. O. & Chait, B. T. Virtual gating and nuclear transport: the hole picture. *Trends Cell Biol.* **13**, 622–628 (2003).
25. Weis, K. Regulating access to the genome: nucleocytoplasmic transport throughout the cell cycle. *Cell* **112**, 441–451 (2003).
26. Hulsmann, B. B., Labokha, A. A. & Gorlich, D. The permeability of reconstituted nuclear pores provides direct evidence for the selective phase model. *Cell* **150**, 738–751 (2012).
27. Beck, M. & Hurt, E. The nuclear pore complex: understanding its function through structural insight. *Nat. Rev. Mol. Cell Biol.* **18**, 73–89 (2017).
28. Frey, S. & Gorlich, D. FG/FxFG as well as GLFG repeats form a selective permeability barrier with self-healing properties. *EMBO J.* **28**, 2554–2567 (2009).
29. Fried, H. & Kutay, U. Nucleocytoplasmic transport: taking an inventory. *Cell Mol. Life Sci.* **60**, 1659–1688 (2003).
30. Conti, E. & Izaurralde, E. Nucleocytoplasmic transport enters the atomic age. *Curr. Opin. Cell Biol.* **13**, 310–319 (2001).
31. Dormann, D. et al. Arginine methylation next to the PY-NLS modulates Transportin binding and nuclear import of FUS. *EMBO J.* **31**, 4258–4275 (2012).
32. Takeuchi, R. et al. Transportin 1 accumulates in FUS inclusions in adult-onset ALS without FUS mutation. *Neuropathol. Appl. Neurobiol.* **39**, 580–584 (2013).
33. Troakes, C. et al. Transportin 1 colocalization with Fused in Sarcoma (FUS) inclusions is not characteristic for amyotrophic lateral sclerosis-FUS confirming disrupted nuclear import of mutant FUS and distinguishing it from frontotemporal lobar degeneration with FUS inclusions. *Neuropathol. Appl. Neurobiol.* **39**, 553–561 (2013).
34. Guo, L. et al. Nuclear-import receptors reverse aberrant phase transitions of RNA-binding proteins with prion-like domains. *Cell* **173**, 677–692.e620 (2018).
35. Twyffels, L., Gueydan, C. & Kruijs, V. Transportin-1 and Transportin-2: protein nuclear import and beyond. *FEBS Lett.* **588**, 1857–1868 (2014).
36. Lu, J. et al. Types of nuclear localization signals and mechanisms of protein import into the nucleus. *Cell Commun. Signal.* **19**, 60 (2021).
37. Fare, C. M., Rhine, K., Lam, A., Myong, S. & Shorter, J. A minimal construct of nuclear-import receptor Karyopherin-beta2 defines the regions critical for chaperone and disaggregation activity. *J. Biol. Chem.* **299**, 102806 (2023).
38. Jafarinia, H., Van der Giessen, E. & Onck, P. R. Molecular basis of C9orf72 poly-PR interference with the beta-karyopherin family of nuclear transport receptors. *Sci. Rep.* **12**, 21324 (2022).
39. Jovičić, A. et al. Modifiers of C9orf72 dipeptide repeat toxicity connect nucleocytoplasmic transport defects to FTD/ALS. *Nat. Neurosci.* **18**, 1226–1229 (2015).
40. Boeynaems, S. et al. Drosophila screen connects nuclear transport genes to DPR pathology in c9ALS/FTD. *Sci. Rep.* **6**, 20877–20877 (2016).
41. Kriachkov, V. et al. Arginine-rich C9ORF72 ALS proteins stall ribosomes in a manner distinct from a canonical ribosome-associated quality control substrate. *J. Biol. Chem.* **299**, 102774 (2023).
42. Schludi, M. H. et al. Distribution of dipeptide repeat proteins in cellular models and C9orf72 mutation cases suggests link to transcriptional silencing. *Acta Neuropathol.* **130**, 537–555 (2015).
43. Schober, P., Boer, C. & Schwarte, L. A. Correlation coefficients: appropriate use and interpretation. *Anesth. Analg.* **126**, 1763–1768 (2018).
44. Liu, F. et al. Proximity proteomics of C9orf72 dipeptide repeat proteins identifies molecular chaperones as modifiers of poly-GA aggregation. *Acta Neuropathol. Commun.* **10**, 22 (2022).
45. Lim, J. & Yue, Z. Neuronal aggregates: formation, clearance, and spreading. *Dev. Cell* **32**, 491–501 (2015).
46. Neumann, M. et al. Ubiquitinated TDP-43 in frontotemporal lobar degeneration and amyotrophic lateral sclerosis. *Science* **314**, 130–133 (2006).
47. Melamed, Z. et al. Premature polyadenylation-mediated loss of stathmin-2 is a hallmark of TDP-43-dependent neurodegeneration. *Nat. Neurosci.* **22**, 180–190 (2019).
48. Ma, X. R. et al. TDP-43 represses cryptic exon inclusion in the FTD-ALS gene UNC13A. *Nature* **603**, 124–130 (2022).
49. Ryan, S., Rollinson, S., Hobbs, E. & Pickering-Brown, S. C9orf72 dipeptides disrupt the nucleocytoplasmic transport machinery and cause TDP-43 mislocalisation to the cytoplasm. *Sci. Rep.* **12**, 4799 (2022).
50. Zhang, K. et al. The C9orf72 repeat expansion disrupts nucleocytoplasmic transport. *Nature* **525**, 56–61 (2015).
51. Dubey, S. K., Maulding, K., Sung, H. & Lloyd, T. E. Nucleoporins are degraded via upregulation of ESCRT-III/Vps4 complex in Drosophila models of C9-ALS/FTD. *Cell Rep.* **40**, 111379 (2022).
52. McLean, J. R. et al. ALS-associated peripherin spliced transcripts form distinct protein inclusions that are neuroprotective against oxidative stress. *Exp. Neurol.* **261**, 217–229 (2014).
53. Nanaura, H. et al. C9orf72-derived arginine-rich poly-dipeptides impede phase modifiers. *Nat. Commun.* **12**, 5301 (2021).
54. Hou, X., Zaks, T., Langer, R. & Dong, Y. Lipid nanoparticles for mRNA delivery. *Nat. Rev. Mater.* **6**, 1078–1094 (2021).
55. Hofweber, M. et al. Phase separation of FUS is suppressed by its nuclear import receptor and arginine methylation. *Cell* **173**, 706–719.e713 (2018).
56. Gittings, L. M. et al. Symmetric dimethylation of poly-GR correlates with disease duration in C9orf72 FTLD and ALS and reduces poly-GR phase separation and toxicity. *Acta Neuropathol.* **139**, 407–410 (2020).

Acknowledgements

We are grateful to the Jefferson Weinberg ALS Center members for their feedback and support throughout the development of this project. The following sources provided funding for this work: National Institutes of Health R21-NS090912 (D.T.), RF1-AG057882 (D.T.), DoD grant AL220064 (D.T.), R01-NS109150 (P.P.); Muscular Dystrophy Association grant 628389 (D.T.); DoD grant W81XWH-21-1-0134 (M.E.C.); RF1-NS114128 (A.H.); Family Strong for ALS & Farber Family Foundation (A.H., P.P., D.T.); R35GM138109 (L.G.), Dr. Ralph and Marian Falk Medical Research Trust (L.G.), Frick Foundation for ALS Research (L.G.)

Author contributions

M.E.C. and D.T. conceived the study, designed the experiments, and wrote and revised the manuscript. D.T. and L.G. supervised all the experiments, provided the resources for the project, and provided critical feedback for the interpretation of the results. M.E.C. performed the live-cell imaging experiments and the statistical analysis. S.S. and L.B.R. performed FRAP experiments and analyzed the live-cell imaging data. V.K. performed the

experiments in mouse tissues, the co-immunoprecipitations, and the TDP-43 localization experiments. B.M.V. managed the animal colony. S. S. M. performed the experiments with human samples. K.K. prepared primary neuronal cultures. A.B. performed Imapris analysis. A.G. performed the experiments in the test tube and conducted data analysis. A.N. designed lentiviral plasmids and produced the virus. P.P. and A.R.H. participate in the conceptualization of the project.

Competing interests

The authors declare no competing interests.

Additional information

Supplementary information The online version contains supplementary material available at <https://doi.org/10.1038/s42003-024-06071-2>.

Correspondence and requests for materials should be addressed to L. Guo or D. Trotti.

Peer review information *Communications Biology* thanks the anonymous reviewers for their contribution to the peer review of this work. Primary Handling Editors: Ibrahim Javed and Manuel Breuer.

Reprints and permissions information is available at <http://www.nature.com/reprints>

Publisher's note Springer Nature remains neutral with regard to jurisdictional claims in published maps and institutional affiliations.

Open Access This article is licensed under a Creative Commons Attribution 4.0 International License, which permits use, sharing, adaptation, distribution and reproduction in any medium or format, as long as you give appropriate credit to the original author(s) and the source, provide a link to the Creative Commons licence, and indicate if changes were made. The images or other third party material in this article are included in the article's Creative Commons licence, unless indicated otherwise in a credit line to the material. If material is not included in the article's Creative Commons licence and your intended use is not permitted by statutory regulation or exceeds the permitted use, you will need to obtain permission directly from the copyright holder. To view a copy of this licence, visit <http://creativecommons.org/licenses/by/4.0/>.

© The Author(s) 2024